**FINAL TECHNICAL REPORT**

Award #05HQGR0076

# BROADBAND GROUND MOTION SIMULATIONS FOR THE PUENTE HILLS THRUST SYSTEM

**Robert Graves**
URS Group Inc.
566 El Dorado Street, 2nd Floor
Pasadena, CA 91101

*Tel: 626-449-7650*
*Fax: 626-449-3536*
*Email: Robert_graves@urscorp.com*

**FINAL TECHNICAL REPORT**

Award #05HQGR0076

# BROADBAND GROUND MOTION SIMULATIONS FOR THE PUENTE HILLS THRUST SYSTEM

**Robert Graves**
URS Group Inc.
566 El Dorado Street, 2nd Floor
Pasadena, CA 91101

*Tel: 626-449-7650*
*Fax: 626-449-3536*
*Email: Robert_graves@urscorp.com*

## Abstract

In recent years, several studies have been conducted with the aim of quantifying the earthquake potential of the Puente Hills fault within Los Angeles basin. The geometry and slip rate of the Puente Hills Blind-Thrust System were defined by Shaw et al. (2002), and four large-slip paleoearthquakes on this system were identified by Dolan et al. (2003). The seismic potential of this fault system was manifested by the 1987 Whittier Narrows earthquake, which occurred on the Santa Fe Springs segment of the Puente Hills blind thrust.

Currently, the 1987 $M_w$ 5.9 Whittier-Narrows and the 1994 $M_w$ 6.7 Northridge earthquakes provide the most relevant analogies to the types of ground motion effects that may be expected in the Los Angeles region during rupture of the Puente Hills fault. These effects include trapping and amplification of basin waves such as that observed in the Los Angeles basin for Whittier-Narrows, and strong up-dip rupture directivity such as that observed for Northridge. Unfortunately, the Whittier-Narrows event was significantly smaller in magnitude than that expected for a Puente Hills rupture ($M_w$ 6.5-7.1), and the Northridge event had its strongest directivity effects channeled into the mountains north of the San Fernando basin, which is opposite of the Puente Hills case where an up-dip rupture will channel directly into the low velocity sediments of the Los Angeles basin.

The objective of this project is to provide quantitative estimates of the ground motions expected from large earthquakes on the Puente Hills blind thrust. Using broadband ground motion simulation procedures, we will quantify the ground motions that could be generated by earthquakes occurring on the Puente Hills blind thrust, taking account of several important ground motion features. These include the effects of forward rupture directivity, which will be strongest in regions (including downtown Los Angeles) that lie above the top edge of the Puente Hills blind thrust; the effects of basin trapped waves, which will be strongest in the Los Angeles basin to the south of the fault; hanging wall effects, which will be strongest in the northern part of the LA basin (including downtown Los Angeles); and the characteristics of ground motions from buried rupture, which appear to be stronger than those of shallow faulting events.

We have extensive experience in the characterization and modeling of these effects in past earthquakes. This includes the analysis of rupture directivity effects from numerous earthquakes

and the development of an empirical model of these effects. We have performed detailed analyses of the strong motion records of the 1994 Northridge and 1999 Chi-Chi Taiwan earthquakes, which provide the most comprehensive data available on the differences in ground motions between footwall and hanging wall sites, and between shallow and buried rupture on thrust faults. We have recently developed an enhanced broadband time history simulation procedure that combines deterministic aspects at low frequencies ($f < 1$ Hz) with stochastic aspects at high frequencies ($f > 1$ Hz). We have also conducted preliminary simulations of the ground motions in the LA basin region for the 1987 Whittier Narrows earthquake using a 3D finite difference methodology that incorporates both a detailed representation of the basin structure as well as the spatial and temporal complexities of finite fault rupture. Since this earthquake occurred on the Puente Hills blind thrust, these ground motions can be regarded as Green's functions that describe the effects of wave propagation in the Los Angeles basin from this source zone.

The goal of our project is to use rigorous seismological modeling of strong ground motions for scenario ruptures of the Puente Hills blind thrust to help assess and quantify the expected ground shaking hazard for such events. Direct products for earthquake loss reduction in southern California from this work include the development of scenario maps of ground motions from large earthquakes on the Puente Hills blind thrust for use in emergency planning and loss estimation, and the development of broadband ground motion time histories and response spectra from large earthquakes on the Puente Hills blind thrust for use in the design and retrofit of structures.

The following paper describes the work conducted in this project. This paper was presented at the 8th National Conference on Earthquake Engineering, San Francisco, CA, April, 2006.

Graves, R. W. and P. G. Somerville (2006). Broadband ground motion simulations for scenario ruptures of the Puente Hills fault, *8th Nat. Conf. Earthquake Engineering*, EERI, San Francisco, CA, paper no. 1052.

# BROADBAND GROUND MOTION SIMULATIONS FOR SCENARIO RUPTURES OF THE PUENTE HILLS FAULT

Robert. W. Graves[1] and Paul. G. Somerville[1]

## ABSTRACT

As a first step towards assessing the potential ground shaking hazard posed by the Puente Hills fault system, we have simulated the response for several earthquake scenarios. These simulations are unprecedented in scope and scale. For each scenario, we compute broadband (0-10 Hz) ground motion time histories at 66,000 sites, covering most of the Los Angeles metropolitan region. We consider three scenarios ranging from $M_w$ 6.7 to $M_w$ 7.2. In all scenarios, strong rupture directivity channels large amplitude pulses of motion directly into the Los Angeles basin, which then propagate southward as basin surface waves. Typically, the waveforms near downtown Los Angeles are dominated by a strong, concentrated pulse of motion. At Long Beach (across the LA basin from the rupture) the waveforms are dominated by late arriving longer period surface waves. The great density of sites used in the calculation allows the construction of detailed maps of various ground motion parameters, as well as animations of the propagating broadband wave field.

## Introduction

Recent studies have identified the seismic potential of the Puente Hills fault system, which lies directly beneath downtown Los Angeles. The geometry and slip rate of the system were defined by Shaw et al. (2002), and four large-slip paleoearthquakes on this system were identified by Dolan et al. (2003). The seismic potential of this fault system was manifested by the 1987 Whittier Narrows earthquake, which occurred on the Santa Fe Springs segment of the Puente Hills blind thrust (Shaw et al., 2002). Figure 1 shows a map view of the Los Angeles region indicating the location of the Puente Hills fault system.

Currently, the 1987 $M_w$ 5.9 Whittier-Narrows and the 1994 $M_w$ 6.7 Northridge earthquakes provide the most relevant analogies to the types of ground motion effects that may be expected in the Los Angeles region during rupture of the Puente Hills fault. These effects include trapping and amplification of basin waves such as that observed in the Los Angeles basin for Whittier-Narrows, and strong up-dip rupture directivity such as that observed for Northridge. Unfortunately, the Whittier-Narrows event was significantly smaller in magnitude than that expected for a Puente Hills rupture ($M_w$ 6.5-7.1) and was thus relatively weak in its

[1]Principal, URS Corporation, Pasadena, CA, 91101

longer period (T > 1 sec) response, and the Northridge event had its strongest directivity effects channeled into the mountains north of the San Fernando basin, which is opposite of the Puente Hills case where an up-dip rupture will channel directly into the low velocity sediments of the Los Angeles basin. This demonstrates the need for event specific ground motion estimates for the Puente Hills system.

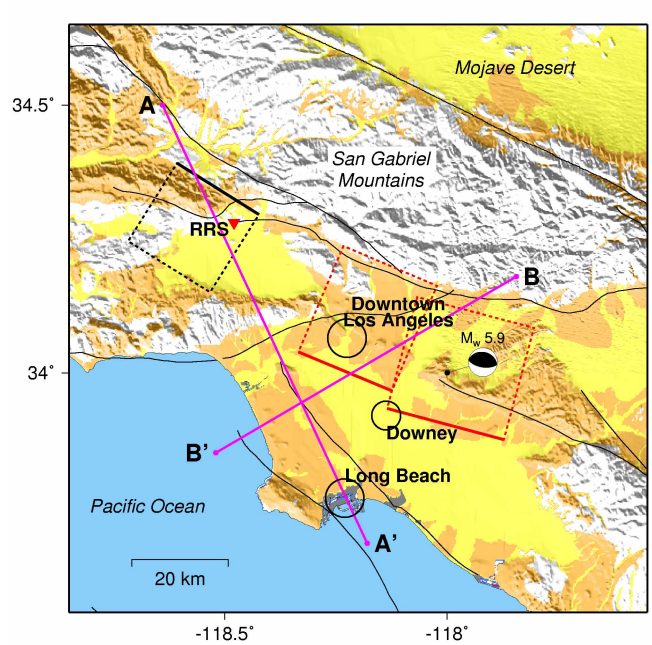


Figure 1. Map of the Los Angeles region indicating the surface projection of the Northridge fault plane (black) and the Puente Hills fault system (red), as well as the location of the Whittier Narrows earthquake. The Los Angeles segment of the PH system lies directly beneath downtown Los Angeles.

Field et al (2005) recently estimated the potential losses generated by Mw 7.2 to Mw 7.5 rupture scenarios for the Puente Hills system. They found that the losses for the Puente Hills events are greater than those experienced during the 1994 Northridge earthquake. This is due to the combination of larger magnitudes and the greater exposure of vulnerable structures to strong shaking for the Puente Hills scenarios. The Field et al (2005) study used empirical ground motion models to estimate shaking levels, and thus did not explicitly incorporate effects such as rupture directivity and basin response for the individual scenarios.

The objective of this study is use full waveform modeling to further quantify the ground motions that could be generated by various scenario earthquakes occurring in the Puente Hills system. To do this, we calculate broadband ground motion time histories for the prescribed scenarios using a hybrid simulation technique. In the sections that follow, we first give a brief overview of the simulation methodology. Next, we provide a description of the fault rupture scenarios, followed by the presentation and discussion of the simulation results.

## Simulation Methodology

The procedure that we will use to simulate broadband ground motions of Puente Hills blind thrust earthquakes is a hybrid procedure that combines a stochastic approach at high frequencies and a deterministic approach at low frequencies. A detailed description of this methodology is given in Graves and Pitarka (2004), which we briefly summarize below.

### Deterministic Methodology (f < 1 Hz)

At low frequencies, the basic calculation is carried out using a 3D viscoelastic finite-

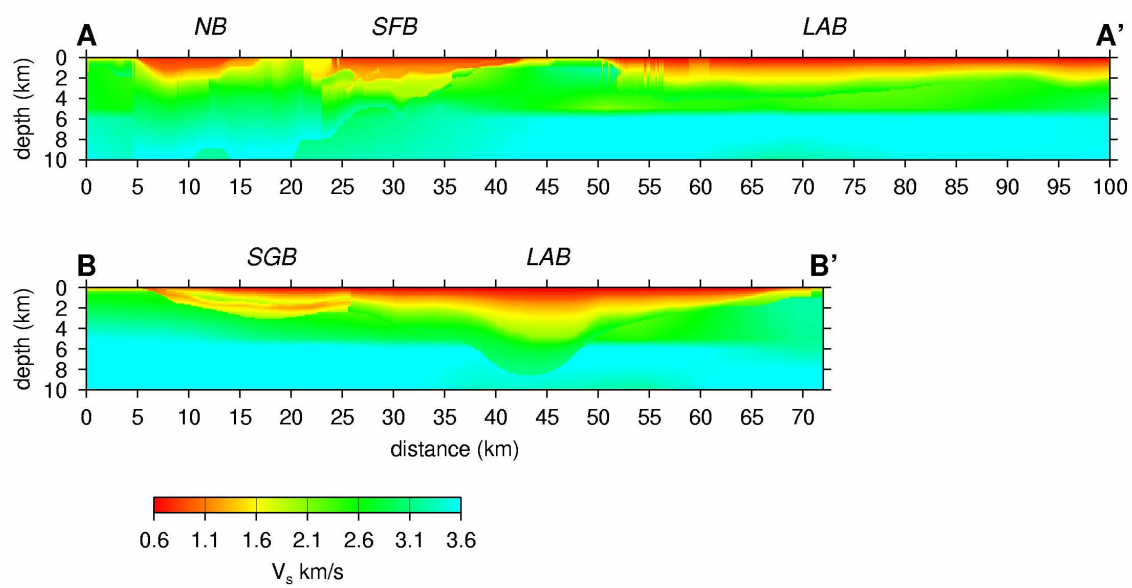


Figure 2. Shear wave velocity cross sections along profiles A-A' and B-B', as indicated in Figure 1. The deep basins are NB = Newhall basin, SFB = San Fernando basin, LAB = Los Angeles basin, SGB = San Gabriel basin (SCEC 3D Community Velocity Model).

difference algorithm, which incorporates both complex source rupture as well as wave propagation effects within arbitrarily heterogeneous 3D geologic structure (Graves, 1996; Pitarka, 1999). Figure 2 shows the complexity of the velocity structure in the Los Angeles region (taken from the SCEC Community Velocity Model). Anealsticity is incorporated using the coarse-grain approach of Day and Bradley (2001). We use a kinematic description of fault rupture, incorporating spatial heterogeneity in slip and rupture velocity by dividing the fault into a number of subfaults. We use a slip velocity function that is constructed using two triangles as shown in Figure 3, following from the dynamic rupture analysis of Guaterri et al. (2003). The parameters controlling this function are:

$$T_r = 1.6\times10^{-9}\cdot M_0^{-1/3}, \quad T_p = 0.2\cdot T_r, \quad h = 0.2\cdot A \tag{1}$$

where $M_0$ is the seismic moment, $T_r$ is the rise time and $A$ is normalized to give the desired final slip. $T_r$ comes from the empirical analysis of Somerville et al. (1999). The rupture initiation time ($T_i$) is determined using the expression

$$T_i = R/V_r - \delta t$$

where $R$ is the rupture path length, $V_r$ is the rupture velocity (set at 80% of $V_s$), and $\delta t$ is a timing perturbation that scales linearly with slip amplitude such that $\delta t = \delta t_0$ where the slip is at its maximum and $\delta t = 0$ where the slip is

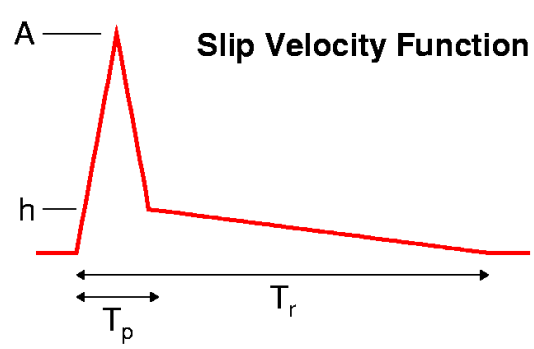


Figure 3. Deterministic slip velocity function.

at the average slip value. We set $\delta t_0 = 0.5\,\text{sec}$. This scaling results in faster rupture across portions of the fault having large slip as suggested by source inversions of past earthquakes (Hisada, 2001).

**Stochastic Methodology (f > 1 Hz)**

The high frequency simulation methodology sums the response for each subfault assuming a random phase, an omega-squared source spectrum and simplified Green's functions. The methodology follows from Boore (1983) with the extension to finite-faults given by Frankel (1995) and Hartzell et al (1999). Each subfault is allowed to rupture with a subfault moment weighting that is proportional to the final static slip amount given by the prescribed rupture model. The final summed moment is then scaled to the prescribed target mainshock moment. The convolution operator of Frankel (1995) scales the subevent rise time to the target rise time. Additionally, this operator also ensures that the result is not dependent on the choice of the subfault dimensions. In our simulations, we fix the subfault stress parameter ($\sigma_p$) at the constant value of 50.

Our formulation allows the specification of a plane layered velocity model from which we calculate simplified Green's functions (GFs) and impedance effects. The GFs are comprised of the direct and Moho-reflected rays, which are attenuated by $1/R_p$ where $R_p$ is the path length traveled by the particular ray. For each ray, we calculate a radiation pattern coefficient by averaging over a range of slip mechanisms and take-off angles.. Anelasticity is incorporated using a travel-time weighted average of the $Q$ values for each of the velocity layers and using a kappa operator set at $\kappa = 0.05$. Finally, gross impedance effects are included using quarter wavelength theory (Boore and Joyner, 1997) to derive amplification functions that are consistent with the specified velocity structure.

**Site Specific Amplification Factors**

Borcherdt (1994) derived empirically based amplification functions with the general form

$$F_x = (V_{site} / V_{ref})^{m_x} \tag{3}$$

where $V_{site}$ is the 30 m travel-time averaged shear wave velocity ($V_s^{30}$) at the site of interest, $V_{ref}$ is the corresponding velocity measure at a reference site where the ground response is known, and $m_x$ is an empirically determined factor. Non-linear effects are included since the $m_x$ decrease as the reference ground response PGA increases.

In both the deterministic and stochastic calculations, we restrict the computational velocity to have $V_s^{30}$ values between 600 and 1000 m/s. This is our $V_{ref}$. The site specific $V_s^{30}$ ($V_{site}$) is obtained from measured or estimated values (e.g., Wills et al, 2000). To obtain an amplification function for a given site velocity, we first determine the short- and mid-period factors from equation (3) using the tabulated $m_x$ from Borcherdt (1994) and the reference PGA from the stochastic response. Next, we construct a smoothly varying function in the frequency

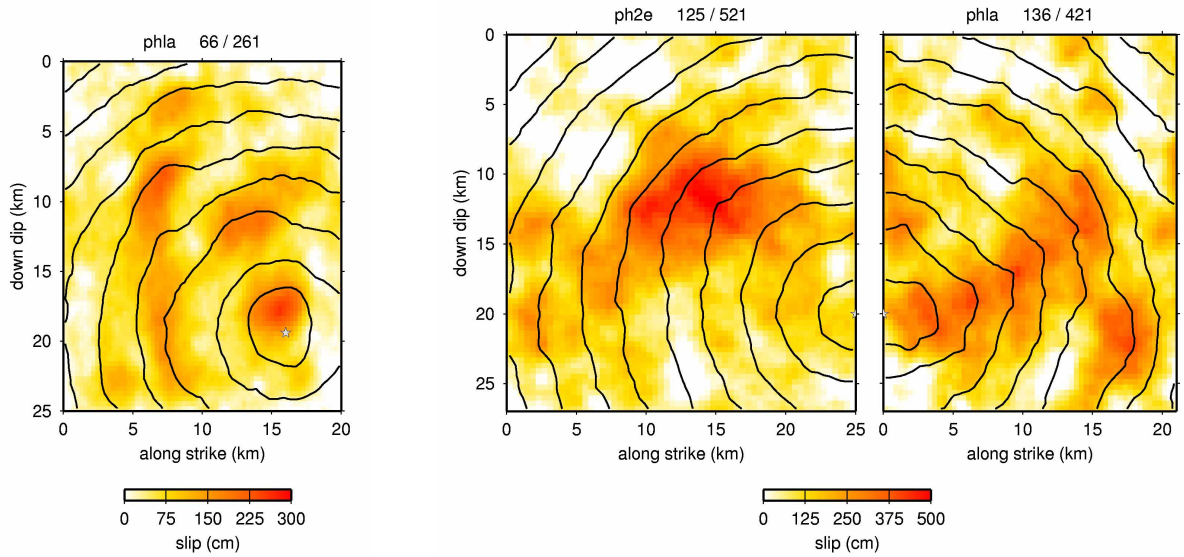


Figure 4. Rupture models for R-1 (left) and R-2 (right). Color shading indicates final slip. Contours show rupture front at 1 s intervals. Star indicates hypocenter. Average slip and maximum slip are indicated at top. Scenario R-3 uses the same slip and hypocenter as R-2.

domain by applying a simple taper to interpolate the factors between the short- and mid-period bands.

## Rupture Scenarios

In this study, we consider three rupture scenarios for the Puente Hills system. The first scenario (R-1) is an $M_w$ 6.7 event that ruptures only the LA segment of the system. The second scenario (R-2) is an $M_w$ 7.2 event that ruptures the entire system (represented as two segments). The third scenario (R-3) uses the same fault segments and slip distribution as R-2; however, the rise time is doubled and the rupture velocity is reduced to 75% of the local Vs. Scenario R-3 is designed to represent a low dynamic stress drop event. Figure 4 plots slip distributions and rupture front contours for scenarios R-1 and R-2. The slip distribution and hypocenter location for R-1 is modeled after the Northridge earthquake (see Hartzell et al., 1996). We have extrapolated the original slip model to a finer discretization using a $K^{-2}$ wavenumber filter. The slip distribution for R-2 is derived using a spatial random field model with a $K^{-2}$ falloff (e.g., Somerville et al., 1999; Mai and Beroza, 2002).

## Ground Motion Simulations

The ground motion simulations for the Puente Hills rupture scenarios are unprecedented in scope and scale. We calculate broadband (0-10 Hz) ground motions over an area 110 km by 150 km, which spans most of the greater Los Angeles metropolitan region. This region is divided into a uniform grid of sites with a spacing of 500 m, yielding a total of 66,000 sites. The low frequency ($f < 1$ Hz) motions are calculated on a fine mesh (h=125 m) using a finite-difference approach, and then sub-sampled to the coarse grid. Nearly 400 million grid points are needed for the FD model and the computations were performed on the HPCC Linux cluster at

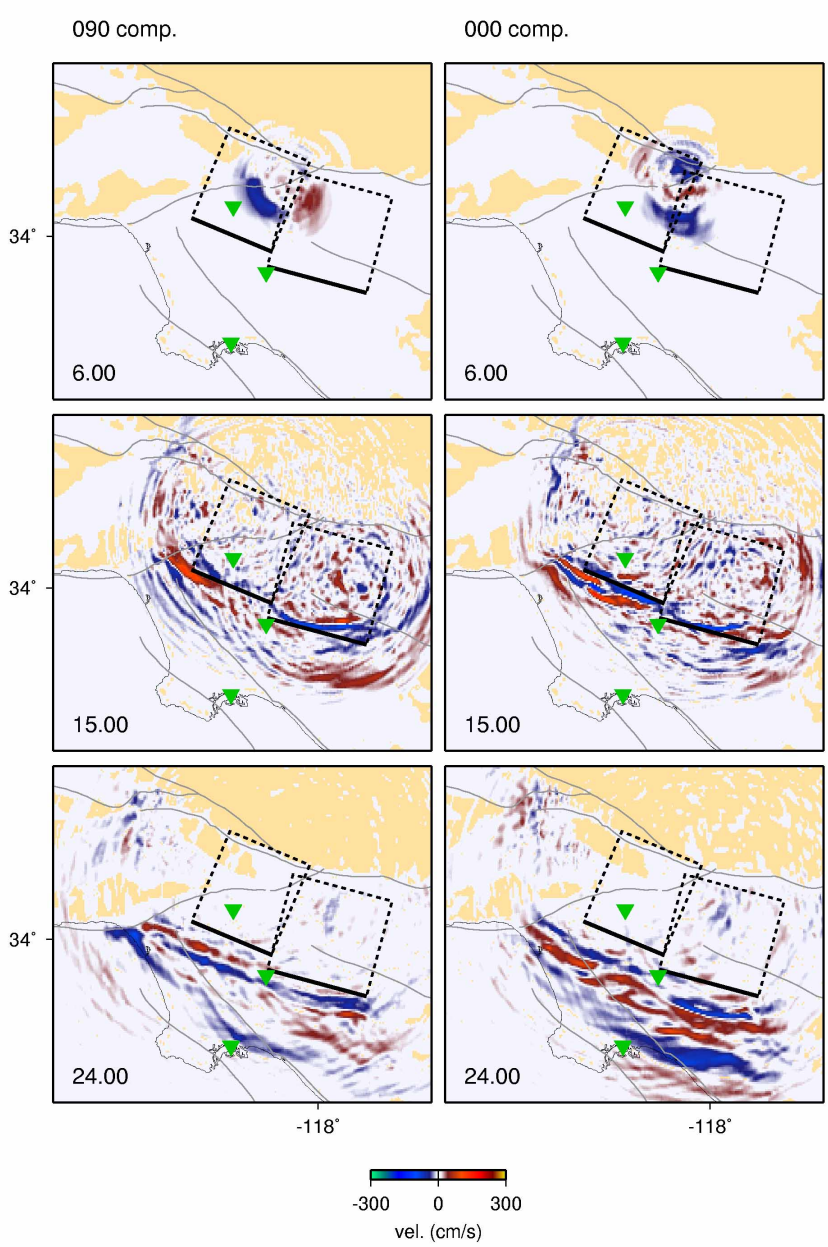


Figure 5. Snapshots of the broadband (0-10 Hz) ground velocity for the E-W (left) and N-S (right) components of motion for scenario R-2. Time (in sec) after earthquake initiation is indicated in the lower left of each panel. The black rectangles indicate the surface projection of the fault planes. Brown shading indicates surface exposure of more consolidated rock, white regions are primarily sediment filled basins. The green triangles denote locations for downtown Los Angeles, Downey and Long Beach.

USC. The high frequency (f > 1 Hz) motions are calculated using the stochastic approach individually for each of the 66,000 locations.

Figure 5 displays snapshots of the propagating broadband velocity wave field for scenario R-2. The complexity of the propagating wave field is readily apparent in these plots.

Strong rupture directivity channels large amplitude pulses of motion directly into the Los Angeles basin, which then propagate southward as basin surface waves. Due to the southward rupture, virtually all of the strongest shaking is directed south from the fault.

This complexity is further apparent in comparing the broadband ground velocity time histories simulated at downtown Los Angeles, Downey and Long Beach for all three rupture scenarios (Figure 6). In all cases, the waveform at Los Angeles is dominated by rupture directivity, which produces a strong, concentrated pulse of motion. At Downey, complexity begins to develop in the waveforms with the appearance of secondary pulses of motion. These pulses are surface waves that are beginning to develop in the basin structure. At Long Beach, which is located across the Los Angeles basin from the rupture, the waveforms are dominated by late arriving longer period surface waves. These surface waves are generated in the near fault region as the direct waves from the rupture are trapped within the sediments of the basin. In general, the characteristics of the motions at each site do not vary greatly for these three scenarios. The most significant effect is the relatively lower amplitude motions generated by scenario R-3.

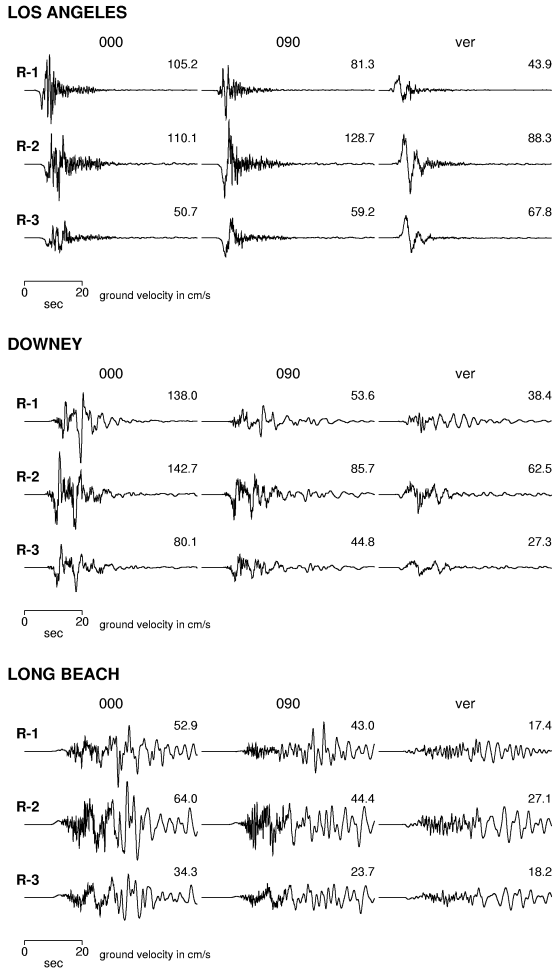


Figure 6: Broadband ground velocity time histories simulated at downtown Los Angeles (top panel), Downey (middle panel) and Long Beach (bottom panel) for the three rupture scenarios.

The great density of sites used in the calculations allows us to construct detailed maps of various ground motion parameters. Examples of these types of ground motion maps are shown in Figure 7, which displays PGA, spectral acceleration at 1 sec and spectral acceleration at 3 sec for each of the three scenarios. At high frequency (PGA), the pattern of ground motions is centered over the fault rupture planes, with the largest motions typically occurring on the hanging wall. At longer periods (1 s and 3 s SA), the strongest motions occur along the top edge of the rupture planes, and are the result of rupture directivity effects. These strong pulses of motion are channeled directly into the soft sediments of the Los Angeles basin and become trapped as basin generated surface waves. These large amplitude surface waves travel

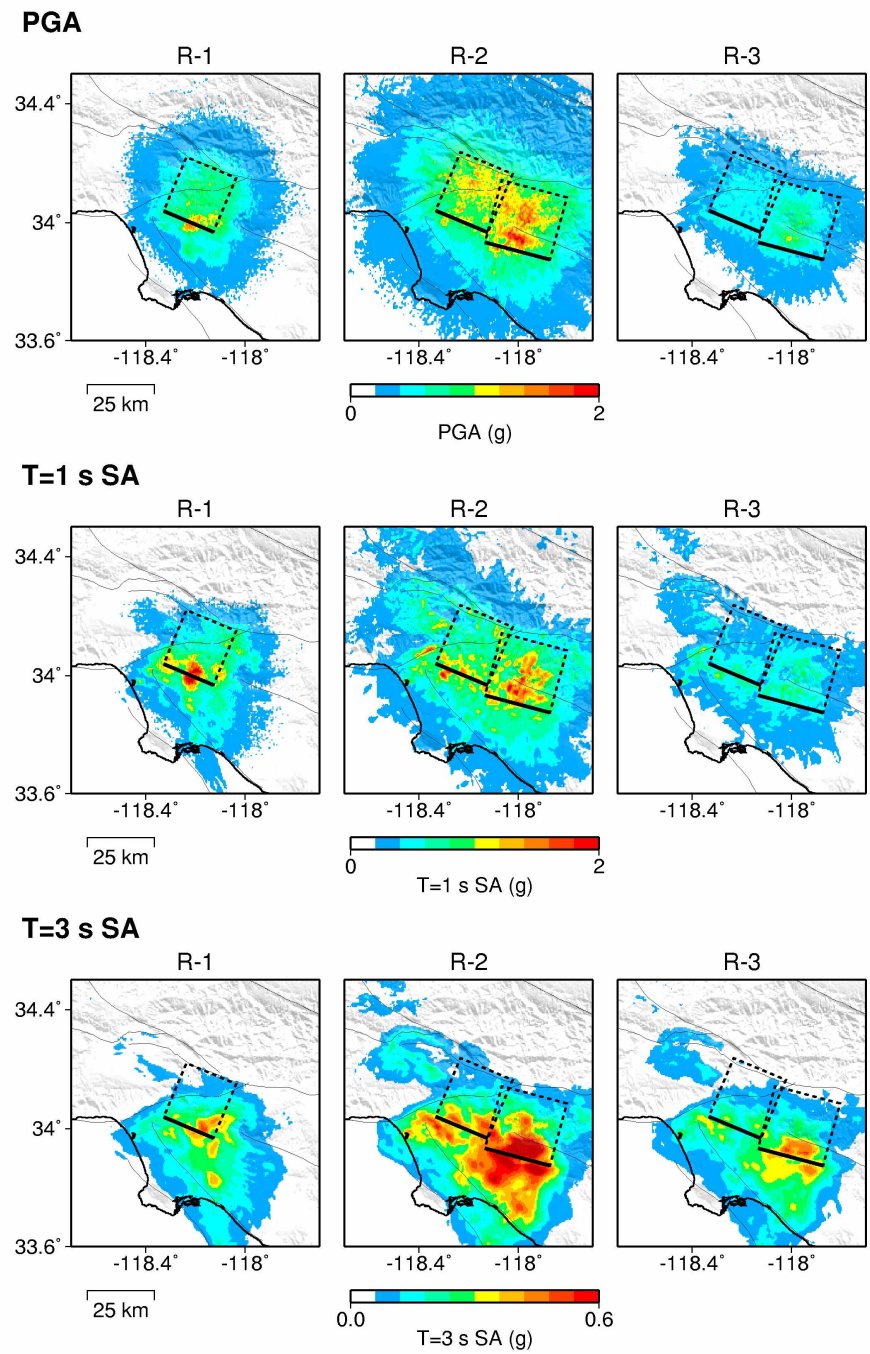


Figure 7. Ground motion maps for PGA (top panels), SA at 1 s (middle panels) and SA at 3 s (bottom panels) for the three rupture scenarios (R-1, R-2 and R-3). The maps in each row are all scaled to the same level to allow direct comparison among the scenarios.

southward across the basin, giving rise to an elongated pattern of elevated, longer period response that extends across the basin.

Scenario R-2 produces the largest overall ground motion levels, followed by scenario R-1 and then R-3. Both scenarios R-1 and R-2 have been modeled as buried rupturing events with relatively short slip rise times (Somerville et al., 1999). The use of a lower rupture velocity and

longer rise time in scenario R-3 (i.e., relatively low dynamic stress drop) significantly reduces the ground motion levels compared to scenario R-2, even though the slip distribution and total moment are the same.

Both scenarios R-2 and R-3 produce larger motions in the eastern portion of the LA basin than in the western portion of the basin. This is due primarily to the prescribed slip distribution, which has the strongest asperity on the eastern fault segment (see Figure 4). We expect that this ground motion pattern would be reversed if the slip distribution for the two segments were switched.

## Conclusions

For all three scenarios, the combination of rupture directivity and basin response produces elevated levels of long-period ground motions throughout the Los Angeles basin region. Although the high frequency motions are less sensitive to these effects, the PGA levels predicted in our simulations are still large, exceeding 1 g in the near source region over the fault planes in all cases. For these scenarios, the most significant variations are seen in the reduced ground motion levels predicted by the low dynamic stress drop event (R-3) compared to both R-1 and R-2. This stresses the need to consider various source parameterizations including constraints provided by dynamic rupture analyses in the assessment of seismic hazard. Obviously, one important aspect of source characterization that we have not fully considered here is the effect of slip distribution. We expect the pattern of ground motions will be dependent on the location of asperities on the fault planes, and further work is needed to more fully quantify and understand the impact of this effect on hazard characterization.

The results presented here illustrate the capabilities of the simulation methodology to produce fully broadband time histories that can be used for seismic hazard assessment or engineering design analyses. We caution that the present results are for only a very limited number of possible scenarios and they should not be used to generally classify the hazard of the Los Angeles basin region. However, our hope is that this type of methodology can be extended to provide a comprehensive treatment of seismic hazard analyses in the near future.

## Acknowledgments

This work has been supported in part by the Southern California Earthquake Center (SCEC) and the external research program of the US Geological Survey (NEHRP).

## References

Boore D. (1983). Stochastic simulation of high frequency ground motions based on seismological models of the radiated spectra, *Bull. Seism. Soc. Am.*, **73**: 1865-1894.

Boore D. and W. Joyner (1997). Site amplification for generic rock sites, *Bull. Seism. Soc. Am.*, **87**, 327-341.

Borcherdt R. (1994). Estimates of site-dependent response spectra for design (methodology and justification), *Earthquake Spectra*, **10**(4), 617-653.

Day S. and C. Bradley (2001). Memory efficient simulation of anelastic wave propagation, *Bull. Seism. Soc. Am.*, **91**, 520-531.

Dolan, J.F., S.A. Christofferson, and J.M. Shaw (2003). Recognition of paleoearthquakes on the Puente Hills Blind Thrust Fault, California. *Science* **300**, 115-118.

Frankel, A. (1995). Simulating strong motions of large earthquakes using recordings of small earthquakes:the Loma Prieta mainshock as a test case, *Bull. Seism. Soc. Am.*, **85**, 1144-1160.

Graves, R.W. (1996). Simulating earthquake ground motions in 3D elastic media using staggered-grid finite-differences, *Bull. Seism. Soc. Am.,* **86**, 1091-1106.

Graves, R. W. and A. Pitarka (2004). Broadband time history simulation using a hybrid approach, *Proc. 13th World Conf. Earthquake Eng.*, Vancouver, Canada, paper no. 1098.

Guatteri M, P. M. Mai, G. Beroza and J. Boatwright (2003). Strong ground motion prediction from stochastic-dynamic source models, *Bull. Seism. Soc. Am.*, **93**, 301-313.

Hartzell S., P. Liu and C. Mendoza (1996). The 1994 Northridge, California earthquake: Investigation of rupture velocity, risetime, and high frequency radiation, *J. Geophys. Res.*, **101**, 20,091-20,108.

Hartzell, S., S. Harmsen, A. Frankel and S. Larsen (1999). Calculation of broadband time histories of ground motion: comparison of methods and validation using strong ground motion from the 1994 Northridge earthquake, *Bull. Seism. Soc. Am.*, **89**, 1484-1504.

Hisada Y. (2001). A theoretical omega-square model considering spatial variation in slip and rupture velocity. part 2. case for a two-dimensional source model, *Bull. Seism. Soc. Am.*, **91**, 651-666.

Mai, P. and G. Beroza (2002). A spatial random field model to characterize complexity in earthquake slip, *J. Geophys. Res.*, **107**(B11), doi:10.1029/2001JB000588.

Pitarka, A. (1999) 3D elastic finite-difference modelling of seismic motion using staggered-grid with non-uniform spacing. Bull. Seism. Soc. Am., **89**,54-68.

Shaw, J.H., A. Plesch, J.F. Dolan, T.L Pratt, and P. Fiore (2002). Puente Hills blind-thrust system, Los Angeles, California, *Bull. Seism. Soc. Am.* **92**, 2946-2960.

Somerville, P.G., K. Irikura, R. Graves, S. Sawada, D. Wald, N. Abrahamson, Y. Iwasaki, T. Kagawa, N. Smith and A. Kowada (1999). Characterizing earthquake slip models for the prediction of strong ground motion. *Seismological Research Letters*, **70**, 59-80.

Wills C., M. Petersen, W. Bryant, M. Reichle, G. Saucedo, S. Tan, G. Taylor and J. Treiman (2000). A site conditions map for California based on geology and shear wave velocity, *Bull. Seism. Soc. Am.*, **90**(6B), S187-S208.